

EELS Tomography in multiferroic nanocomposites: from spectrum images to the spectrum volume (Supplementary information)

Lluís Yedra,^{*a,b} Alberto Eljarrat,^a José Manuel Rebled,^{a,c} Lluís López-Conesa,^a Nico Dix,^c Florencio Sánchez,^c Sònia Estradé,^{a,b} and Francesca Peiró^a

5

Experimental

The BiFeO₃ – CoFe₂O₄ epitaxial nanocomposite was deposited on a LaNiO₃-buffered LaAlO₃ (001) substrate by pulsed laser deposition. Detailed information about preparation conditions and properties is reported elsewhere¹.

EELS and HAADF were obtained in a JEOL JEM2010F coupled to a Gatan GIF spectrometer, operated at 200 kV, with a high resolution ultra narrow pole piece. The sample was prepared in a nanoneedle shape by Focused Ion Beam (FIB) in a FEI Strata 235 Dual Beam System. The structure of the material can be observed in Figure S1. The nanoneedle was attached to the usual Omniprobe grid, only shortened at both ends to keep the maximum dimension below 1.5 mm in order to fit to a special sample holder (Fishione 2030 ultra-narrow gap tomography holder).

The tilt series of the first experiment (refer to Figure 2(a-c) and the corresponding passage of the main text) ranged from -65.7° to 61.8°, at tilt steps of 3°. For each tilt step a spectrum image (SI) and a HAADF image were acquired, ending up with 44 SI consisting in 14x27 single spectra each and 2.8 nm per pixel. Every 14 spectra (one row of the SI), sample drift was corrected using cross correlation in a HAADF survey image and exposure time was 1 second per spectrum.

The second experiment (refer to Figure 2(d-f) and the corresponding passage of the main text) ranged from -64° 4 to 70°, at tilt steps of 2°. The resulting data consisted in 67 SI and HAADF images of 33x39 pixels with a resolution of 2.5 nm per pixel. In this second experience, measure times were reduced to 0.8 seconds and sample drift was also corrected once per row. Tilt angles were externally measured using an external clinometer for higher precision. Spectra were acquired with a collection angle of 20 mrad from 424 to 936 eV, with 0.5 eV per channel for both experiments. Lower acquisition times were preferred in this second experiment, as the amount of spectra to acquire was extremely high and sample damage should be prevented. However, a further decrease in the acquisition times was found to be detrimental because the signal could not be properly separated from the noise in the subsequent multivariate statistical analysis. In this range, O K edge (532 eV), Fe L_{2,3} edge (708 eV) and La M_{4,5} edge (832 eV) were clearly visible. Other expected edges on this range, such as Co L_{2,3} (779 eV) and Ni L_{2,3} (855 eV) were hardly visible. It can be explained by the lower concentration of these transition metals, the proximity to

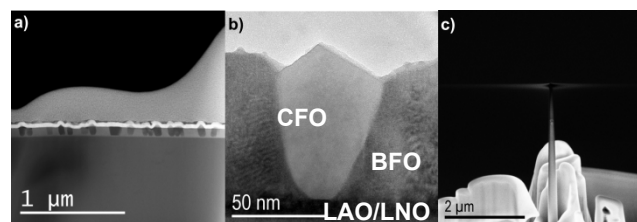


Figure S1: Sample preparation. a) HAADF STEM image of the multiferroic nanocomposite, where the CFO columns can be observed, b) CFO nanocolumn in BFO and c) SEM image of the needle shaped sample prepared in the FIB

the tail of previous edges (as the sample is about 80 nm thick and thus the signal to background is reduced), low acquisition times, which lower the signal to noise ratio and low brightness (intensity current) of the used TEM.

Data analysis

The spectra present a low signal noise ratio, which is due to the low acquisition times, so in a first step the noise level was reduced by taking advantage of Multivariate Analysis (MVA). Using Hyperspy^{2, 3}, a Python based EELS analysis toolbox, the energy drift of the data was corrected using the region around O K edge. Afterwards, weighted principal component analysis (PCA) was applied, assuming a dominant Poissonian noise in the weighting.

PCA is a spectral analysis technique consisting on finding a new parametric model for the dataset, where every spectrum can be described as a weighted sum of a finite number of components and noise. Three assumptions are made: (i) that the problem is linear, (ii) that signal has higher variance than the noise and (iii) component orthogonality. The signals are separated according to their variance⁴, therefore, by keeping only higher variance components and discarding the noise an enhanced signal-to-noise ratio can be obtained. An example is shown in Figure S2 for the first experiment dataset, where the difference in the same spectrum before and after PCA noise reduction is shown for one single spectrum at -38.2° tilt. In the first experiment, 6 components were retained, while in the second experiment 4 of them were kept for further analysis. In both cases, the choice is made observing the components and keeping only those with relevant signal. In Figure S4, The scree plots and the first rejected component are shown for the first experiment (a) and the second

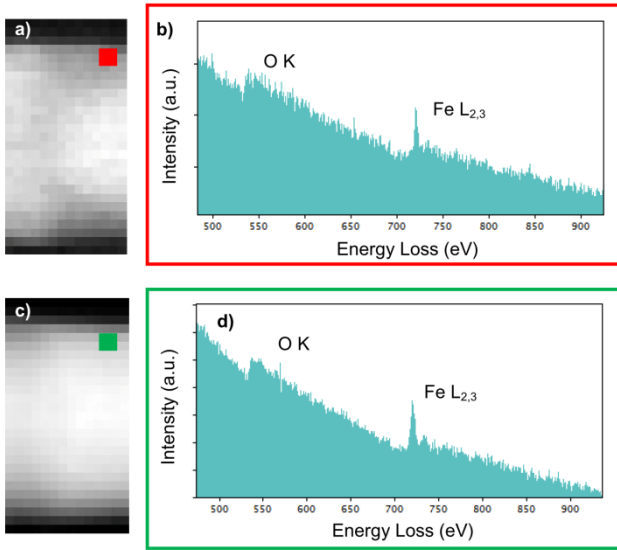


Figure S2: a) spectrum image at -38.2° tilt with b) extracted spectrum from the area marked with the red square. c) Spectrum image after PCA noise reduction and d) extracted spectrum from the region marked with the green square. There is a clear increase in signal to noise ratio in the data after PCA.

(b). The signals in the rejected components can be linked to energy instabilities in the acquisition, and do not offer further information to the spatial distribution of the elements.

In addition to the core-loss maps, high angle annular dark field (HAADF) signal was coacquired for each spectrum. HAADF signal was used to measure spatial drift between images and to correct for tilt axis. Moreover, HAADF is the most used signal in electron tomography, so the reconstruction can be used for comparison reasons. Survey images, also based on HAADF are also reconstructed, as they have, nonetheless, better spatial resolution and offer the view of a larger area of the nanoneedle. We have used Hyperspy data analysis software to perform despiking and alignment processing the hyperspectral datacube resulting from the stacking of the spectrum images (SI) from each projection^{2, 3}. The same software was used for the assessment of the multivariate analysis procedure: weighted principal components analysis (PCA) through the singular value decomposition (SVD) algorithm. Finally, PCA followed by blind source separation (BSS) was performed using the Bayesian Linear Unmixing software by N. Dobigeon⁵. PCA is applied first to reduce the number of components, as the BSS procedures are much more computer intensive. In this last data processing, the constraints are the number of components, their non-negative nature and that maps should be limited to proportions. As explained in ⁶, we established the number of separated components to 4, chosen the N-FINDR geometrical algorithm for generating the prior estimations and let a maximum number of unmixing iterations of 50.

Edge intensities extraction method consisted in removing the background previous to each edge approximating it by an inverse power law and then integrating the area under the edges for 40 eV (see Figure S3). The extracted maps were oversampled using a bipolar interpolation, so the alignment and reconstruction software could perform cross-correlations with better accuracy. IMOD⁷ and Inspec3D were the chosen software for image and

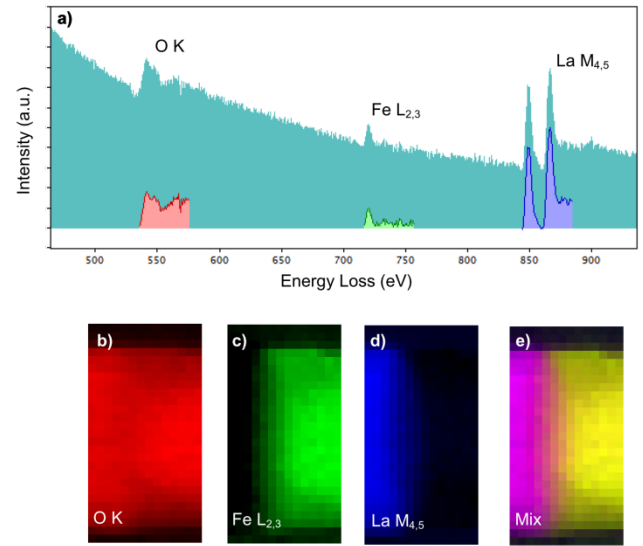


Figure S3: Extraction of edge intensities in the first experiment a) single spectrum from SI after PCA treatment at -38.2° . The shaded areas represent the integrated area of the edges after background subtraction for oxygen (in red), iron (in green) and lanthanum (in blue). Maps of extracted edge intensities for b) O K, c) Fe L_{2,3} and d) La M_{4,5} are shown combined in e).

tilt axis alignment and reconstruction. IMOD was used in the first experiment (which contains less details) for spatial drift, as it was found more suitable for images obtained from EELS with few details, while the second experiment was corrected directly in Inspec3D. Spatial drift was measured in HAADF coacquired signal and then applied to the core-loss signals to correct SI spatial position. SIRT algorithm⁸ with 30 iterations was used for the reconstruction in the first experiment dataset and 20 iterations were used in the second one. Avizo imaging software was used for the final segmentation and visualization of the data.

In order to obtain a 3D reconstruction of a signal coming from an object by means of tomographic methods, this signal must behave monotonically with a property of the object⁹, which is the so-called projection requirement. For extracted intensities, the use in tomography can be justified as follows:

The signal for each element is given by the equation:

$$I_k^A(\beta, \Delta) = N^A \sigma_k^A(\beta, \Delta) I_t(\beta) e^{-\lambda} \quad (1)$$

where I_k^A is the edge intensity of a k transition for an element A, integrated over an angle β and in the energy range Δ , N^A is the areal density of element A (concentration times thickness), σ_k^A is the k ionization partial cross-section of element A, I_t the total transmitted beam intensity, t is the thickness and λ is the inelastic mean free path.

This expression relies on the assumption that there is only one scattering event of core-loss nature. Single scattering distribution of the signal is predominant where thickness is lower than the inelastic mean free path, which in our case is over 100 nm¹⁰. Adding the influence of the plasmon losses does not change the relationship in equation 1. Plasmon losses cause the intensities of the edges to be shifted to higher energies. As long as a single plasmon excitation dominates valence scattering and that the integration window is big enough, the extracted signal continues to behave monotonically. In our case, we will assume that in our

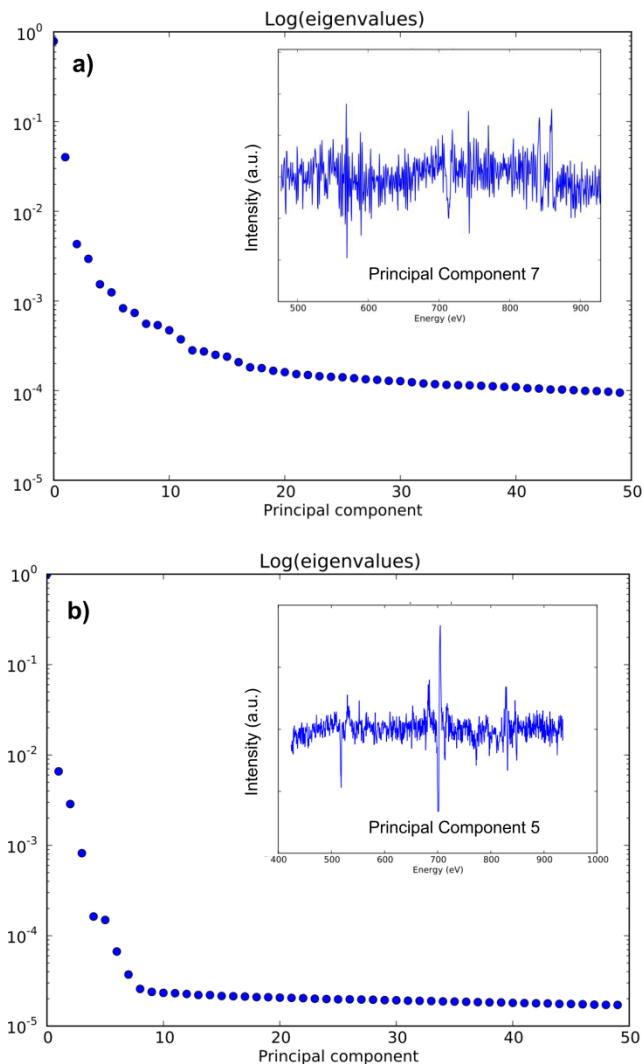


Figure S4: a) Scree plot from the PCA of the first experiment. The first rejected component is shown in the inset. b) Scree plot for the second experiment, also showing the first rejected component. The rejected components contained mostly noise and some instabilities in energy, so their contribution was not considered relevant.

range of thickness this term does not affect the monotonicity of the signal.

Some other effects can make the signal fail to fulfill the projection requirement, such as diffraction contrast, which lowers the overall intensity of the spectra. In our dataset, the measured total intensity of the SI did not change substantially over the tilting process, thus the influence of diffraction contrast is of no importance. In summary we can consider that the extracted signal changes monotonically with the thickness and the density of each element in our sample as shown in Figure 3 of the main text.

Notes and references

^a Laboratory of Electron Nanoscopies (LENS)- MIND/IN2UB, Dept. d'Electrònica, Universitat de Barcelona, C/Martí i Franquès 1, 08028 Barcelona, Spain; E-mail: llyedra@el.ub.edu

^b CCI, Scientific and Technological Centres, Universitat de Barcelona, C/Lluís Solé i Sabaris 1, 08028 Barcelona, Spain.

^c Institut de Ciència de Materials de Barcelona (ICMAB-CSIC), Campus de la UAB, 08193 Bellaterra, Spain

- 1 N. Dix, R. Muralidharan, J. Rebled, S. Estrade, F. Peiro, M. Varela, J. Fontcuberta and F. Sanchez, *Acs Nano*, 2010, **4**, 4955-4961 (DOI:10.1021/nn101546r).
- 2 R. Arenal, F. de la Peña, O. Stéphan, M. Walls, M. Tencé, A. Loiseau and C. Colliex, *Ultramicroscopy*, 2008, **109**, 32-38 (DOI:DOI: 10.1016/j.ultramic.2008.07.005).
- 3 F. de la Peña, M. - Berger, J. - Hochepped, F. Dynys, O. Stephan and M. Walls, *Ultramicroscopy*, 2011, **111**, 169-176 (DOI:DOI: 10.1016/j.ultramic.2010.10.001).
- 4 R. N. Cochran and F. H. Horne, *Anal. Chem.*, 1977, **49**, 846-853 (DOI:10.1021/ac50014a045).
- 5 N. Dobigeon, S. Moussaoui, M. Coulon, J. Tourneret and A. O. Hero, *Ieee Transactions on Signal Processing*, 2009, **57**, 4355-4368 (DOI:10.1109/TSP.2009.2025797).
- 6 N. Dobigeon and N. Brun, *Ultramicroscopy*, 2012, **120**, 25-34 (DOI:10.1016/j.ultramic.2012.05.006).
- 7 J. R. Kremer, D. N. Mastrorade and J. R. McIntosh, *J. Struct. Biol.*, 1996, **116**, 71-76 (DOI: 10.1006/jsbi.1996.0013).
- 8 P. Gilbert, *J. Theor. Biol.*, 1972, **36**, 105-117 (DOI:DOI: 10.1016/0022-5193(72)90180-4).
- 9 P. W. Hawkes, *The Electron Microscope as a Structure Projector*, Springer New York, 2006.
- 10 Egerton R. F., *Electron Energy-Loss Spectroscopy in the Electron Microscope*, Springer, New York, 2011.